[18] Press, W. H., Teukolsky, S. A., Vetterling, W. T., and Flannery, B. P.
Numerical Recipes in C, The Art of Scientific Computing (2nd ed.).
New York: Cambridge University Press, 1992.

[19] Abramowitz, M. and Stegun, I.
Handbook of Mathematical Functions (9th printing).
New York: Dover, 1972.

[20] Pastor, D. and Amehraye, A.
Algorithms and applications for estimating the standard deviation of AWGN when observations are not signal-free.
Journal of Computers, **2**, 7 (Sept. 2007).

[21] Golliday, C.
Data link communications in tactical air command and control systems.
IEEE Journal on Selected Areas in Communications, **3**, 5 (1985), 1985.

[22] Haas, E.
Aeronautical channel modeling.
IEEE Transactions on Vehicular Technology, **51**, 2 (Mar. 2002), 254–264.

Monopulse MIMO Radar for Target Tracking

We propose a multiple input multiple output (MIMO) radar system with widely separated antennas that employs monopulse processing at each of the receivers. We use Capon beamforming to generate the two beams required for the monopulse processing. We also propose an algorithm for tracking a moving target using this system. This algorithm is simple and practical to implement. It efficiently combines the information present in the local estimates of the receivers. Since most modern tracking radars already use monopulse processing at the receiver, the proposed system does not need much additional hardware to be put to use. We simulated a realistic radar-target scenario to demonstrate that the spatial diversity offered by the use of multiple widely separated antennas gives significant improvement in performance when compared with conventional single input single output (SISO) monopulse radar systems. We also show that the proposed algorithm keeps track of rapidly maneuvering airborne and ground targets under hostile conditions like jamming.

I. INTRODUCTION

A radar transmitter sends an electromagnetic signal which bounces off the surface of the target and travels in space towards the receiver. The signal processing unit at the receiver analyzes the received signal to infer the location and properties of the target. When the electromagnetic signal reflects from the surface of the target, it undergoes an attenuation which depends on the radar cross section (RCS) of the target. This RCS varies with the angle of view of the target. We can exploit these angle dependent fluctuations in the RCS values to provide spatial diversity gain by employing multiple distributed antennas [1–7]. When viewing the target from different angles simultaneously, the angles which result in a low RCS value are compensated by the others which have a higher RCS, thereby leading to an overall improvement in the performance of the radar system. This is the motivation for using multiple input multiple output (MIMO) radar with widely separated antennas. Along with widely separated antenna

Manuscript received October 5, 2009; revised February 8 and May 14, 2010; released for publication July 3, 2010.

IEEE Log No. T-AES/47/1/940063.

Refereeing of this contribution was handled by F. Gini.

This work was supported by the Department of Defense under the Air Force Office of Scientific Research MURI Grant FA9550-05-1-0443 and ONR Grant N000140810849.

0018-9251/11/$26.00 © 2011 IEEE

configuration, MIMO radar has also been suggested for use in a colocated antenna configuration [8, 9]. Such a system exploits the flexibility of transmitting different waveforms from different elements of the array. In this paper, we only deal with MIMO radar in the context of distributed antennas.

Most of the tracking radars have separate range tracking systems apart from angle tracking systems. The range tracking system keeps track of the range (distance) of the target and sends only signals coming from the desired range gate to the angle tracking system [10]. The range tracker would have an estimate of the time intervals when the target returns are expected. The focus of this paper however is on the angle tracking system which is primarily implemented using either of two main mechanisms, sequential lobing and simultaneous lobing [10–12]. In both these mechanisms, we project the radar beams slightly to either side of the radar axis in both the angular dimensions (azimuth and elevation). We compare the received signals in each of these beams to keep track of the angular position of the target. To perform this comparison, the system computes a ratio which is a function of the signals received through these beams. This ratio is called monopulse ratio [11]. In [13]–[17], the statistical properties of this ratio are studied in detail under different scenarios.

In sequential lobing, as the name suggests, we carry out this procedure in a sequential manner by alternating between the different beams from one pulse to another. However, in simultaneous lobing, we generate all the beams at the same time. Simultaneous lobing is also called as monopulse. If there are heavy fluctuations in the target returns from one time instant to another, sequential lobing suffers from a degradation in performance whereas monopulse is immune to these fluctuations because we measure the signals coming from all the beams at the same time [10–12]. Apart from this, sequential lobing also suffers from a reduction in the data rate because we need multiple pulses to receive the data from all the beams. However, the advantages offered by simultaneous lobing come at the cost of increased complexity because we need additional hardware to generate the two beams at the same time.

Most modern radars use monopulse processors and this topic is well studied in the literature [18–22]. In [23] an overview of monopulse estimation is presented. There are two types of monopulse tracking radars in use; amplitude-comparison and phase-comparison. In amplitude-comparison monopulse, the beams originate from the same phase center whereas the beams in a phase-comparison monopulse system are parallel to each other and originate from slightly shifted (extremely small when compared with the beamwidth) phase centers [12]. Essentially, the signals received from both the beams have the same phase in amplitude-comparison monopulse and they differ only in the amplitude. However, for phase-comparison monopulse systems, the exact opposite is true [24]. Stochastic properties of the outputs of both these systems were studied earlier [25]. In the rest of this paper, whenever we refer to monopulse, we mean amplitude-comparison monopulse.

Apart from active systems, there are also passive systems in the literature that consider the problem of localization using the bearing estimates [26–28]. See also [29, ch. 3]. References [27] and [28] consider only stationary targets in their results. Also, [26]–[28] do not use monopulse processing at the receivers. In this paper, we propose a radar system that combines the advantages of monopulse and distributed MIMO radar (see also [30]). It provides the spatial diversity offered by MIMO radar with widely separated antennas and is also immune to highly fluctuating target returns just like any monopulse tracking radar. To the best of our knowledge, we are the first to propose such an active radar system for target localization. We have considered rapdily maneuvering moving targets and also considered hositle conditions like jamming.

The rest of this paper is organized as follows. In Section II we propose a monopulse MIMO radar system and describe its structure in detail. In Section III we describe the signal model of our proposed system. In Section IV we propose a tracking algorithm for this monopulse MIMO radar system. We describe the various steps involved in tracking the location of the target. In Section V we use numerical simulations to demonstrate the improvement in performance offered by this proposed system over conventional single input single output (SISO) monopulse systems. We also show that the proposed algorithm keeps track of an airborne target even when it maneuvers quickly and changes directions. We deal with a scenario in which an intentional jamming signal tries to degrade the performance of the tracker and demonstrate that the algorithm does not lose track of the target even in such a difficult scenario. We show the advantages of using simultaneous lobing (monopulse) in our system as opposed to sequential lobing which fails to keep track of the target in this jamming scenario. Further, we demonstrate that the proposed radar system efficiently keeps track of a ground target that changes directions at sharp angles. Finally, in Section VI, we conclude this paper.

II. SYSTEM DESCRIPTION

In this section we begin with a brief description of our proposed system. Fig. 1 gives the basic structure of our monopulse MIMO radar system. The system has M transmit antennas and N receive antennas. The different transmitters illuminate the target from multiple angles and the reflected signals from the

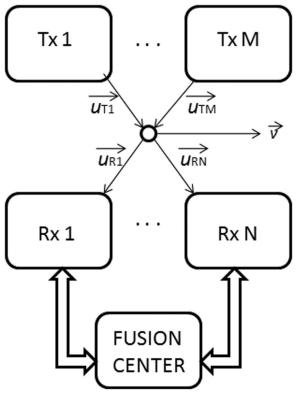

Fig. 1. Our proposed monopulse MIMO radar system.

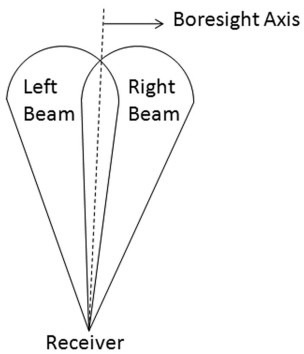

Fig. 2. Overlapping monopulse beams at one of the receivers.

surface of the target are captured by widely separated receivers. All the receivers are connected to a fusion center which can be a separate block by itself or one of the receivers can function as the fusion center. Each of the receivers generates two overlapping receive beams on either side of the boresight axis (see Fig. 2). Before initializing the tracking process, the fusion center makes the boresight axes of all the receivers point towards the same point in space (see Fig. 3). The fusion center has knowledge of the exact locations of all the transmit and receive antennas and hence it can direct the receivers to align their respective axes accordingly.

In this paper we assume that the target moves only in the azimuth plane scanned by these beams. However, we can easily extend this to the other angular dimension (elevation) without loss of generality by adding the extra beams. We compare the signals arriving through the two beams at each of the receivers in order to update the estimate of the angular position of the target. If the target is present to the left side of the boresight axis, then we expect the power of the signal from the left beam to be higher when compared with that from the right beam in an ideal noiseless scenario. After comparison of the signals, each receiver updates its angular estimate of the target location by appropriately moving the boresight axis. All the receivers send their new local angular estimates to the fusion center. The fusion

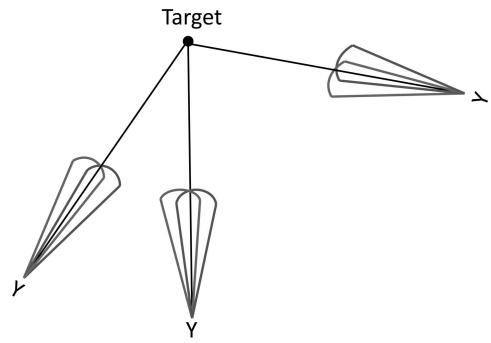

Fig. 3. Monopulse MIMO radar receivers.

center makes use of all the information sent to it and makes a final global decision on the location where the target could be present. It instructs all the receivers to align their boresight axes towards this estimated target location. After this processing, the receivers get ready for the next iteration. We give the details of how these local and global estimates are updated in Section IV.

III. SIGNAL MODEL

A. Transmitted Waveforms

As mentioned in the previous section, we assume there are M widely separated transmit antennas. Let $\tilde{s}_i(t)$, $i = 1,\ldots,M$, denote the complex baseband waveform transmitted from the ith antenna. Therefore, after modulation, the bandpass signal emanating from the ith transmit antenna is given as

$$s_i(t) = \mathrm{Re}\{\tilde{s}_i(t)e^{j2\pi f_c t}\} \tag{1}$$

where $\mathrm{Re}\{\cdot\}$ denotes the real part of the argument, $j = \sqrt{-1}$, and f_c denotes the carrier frequency. We assume that $\tilde{s}_i(t)$, $\forall i = 1,\ldots,M$ are narrowband waveforms with pulse duration T s. We repeat each of these pulses once every T_R s. We do not impose any further constraints on these waveforms. Especially note that we do not need orthogonality between the different transmitted waveforms unlike conventional MIMO radar with widely separated antennas. As we see later in the paper, the reason for this is that we do not need a mechanism to separate these waveforms at the receivers. We process the sum of the signals coming from different transmitters collectively without separating them. This is another advantage of the proposed system because the assumption that the waveforms remain orthogonal for different delays and Doppler shifts is unrealistic. In Section V (numerical results), we consider rectangular pulses.

B. Target and Received Signals

We assume a far-field target in our analysis. Further, we assume that the target is point-like with its RCS varying with the angle of view. Hence, the signals coming from different transmitters undergo

different attenuations before they travel to the receivers. Let $a_{ik}(t)$ denote the complex attenuation factor due to the distance of travel and the target RCS for the signal transmitted from the ith transmitter and reaching the kth receiver and τ_{ik} is the corresponding time delay. Note that for a colocated MIMO system, $a_{ik}(t)$ for different transmitter-receiver pairs will be the same because all the antennas will be viewing the target from closely-spaced angles. Different models have been proposed in the literature to model the time-varying fluctuations in these attenuations $a_{ik}(t)$ [31–33]. Some of these models incorporate pulse-to-pulse fluctuations, scan-to-scan fluctuations, etc. These correspond to fast moving and slow moving targets, respectively. In our numerical simulations, we consider a rapidly fluctuating scenario where these attenuations keep varying from one pulse instant to another because of the motion of the target. We assume $a_{ik}(t)$ to be constant over the duration of one pulse. These attenuations $a_{ik}(t)$ are not known at the receivers. The complex envelope of the signal reaching towards the kth receiver is the sum of all the signals coming from different transmitters

$$\tilde{y}_k(t) = \sum_{i=1}^{M} a_{ik}(t)\tilde{s}_i(t-\tau_{ik}). \tag{2}$$

Hence, the actual bandpass signal arriving at the kth receiver is

$$y_k(t) = \sum_{i=1}^{M} \mathrm{Re}\{a_{ik}(t)\tilde{s}_i(t-\tau_{ik})e^{j2\pi f_c(t-\tau_{ik})}\}. \tag{3}$$

So far, we have assumed the target to be stationary. When the target is moving, we modify the above equation to include the Doppler effect. Under the narrowband assumption for the complex envelopes of the transmitted waveforms, and further assuming the target velocity to be much smaller than the speed of propagation of the wave in the medium, the Doppler would not affect the component $a_{ik}(t)\tilde{s}_i(t-\tau_{ik})$ and it shows up only in the carrier component, transforming the signal to

$$y_k(t) = \sum_{i=1}^{M} \mathrm{Re}\{a_{ik}(t)\tilde{s}_i(t-\tau_{ik})e^{j2\pi(f_c(t-\tau_{ik})+f_{\mathrm{D}ik}(t-\tau_{ik}))}\} \tag{4}$$

where $f_{\mathrm{D}ik}$ is the Doppler shift along the path from the ith transmitter to the kth receiver,

$$f_{\mathrm{D}ik} = \frac{f_c}{c}(\langle \vec{\mathbf{v}}, \vec{\mathbf{u}}_{\mathrm{R}k}\rangle - \langle \vec{\mathbf{v}}, \vec{\mathbf{u}}_{\mathrm{T}i}\rangle) \tag{5}$$

where $\vec{\mathbf{v}}, \vec{\mathbf{u}}_{\mathrm{T}i}, \vec{\mathbf{u}}_{\mathrm{R}k}$ denote the target velocity vector, unit vector from the ith transmitter to the target and the unit vector from the target to the kth receiver, respectively; $\langle , \rangle$ is the inner product operator, and c is the speed of propagation of the wave in the medium. Equation (4) is valid only when the target is moving with constant velocity. It is reasonable to assume uniform motion within any given processing interval because the typical duration of a processing interval is very small. If the target is accelerating and if the complex envelope is wideband, more detailed expressions can be derived using the theory in [34]–[37]. Note that the Doppler shifts $f_{\mathrm{D}ik}$ are not known at the receivers.

C. Beamforming

The receive beams are generated using Capon beamformers [38, 39]. Capon beamformer is the minimum variance distortionless spatial filter. In other words, it minimizes the power of noise and signals arriving from directions other than the specific direction it was designed for. Each receiver generates two beams located at the same phase center using two linear arrays. Each array has L elements, each separated by a uniform distance of $\lambda/2$, where $\lambda = c/f_c$ is the wavelength corresponding to the carrier. Under the given antenna spacing, the steering vector of the beamformers becomes

$$\mathbf{d}(\theta, f) = \left[1, e^{-j\pi(f\lambda/c)\cos\theta}, \ldots, e^{-j(L-1)\pi(f\lambda/c)\cos\theta}\right]^{\mathrm{T}} \tag{6}$$

where $[\cdot]^{\mathrm{T}}$ denotes the transpose. Let θ_k be the angle between the approaching plane wave and the two linear arrays at the kth receiver (see Fig. 4). The received signals are first demodulated before passing through the two beamformers. Define the outputs of the two beamformers as $y_k^{\mathrm{l}}(t)$ and $y_k^{\mathrm{r}}(t)$, where the superscripts l and r correspond to the left and the right beams, respectively (see Fig. 2). Also, let $\mathbf{w}_k^{\mathrm{l}} = [w_{k1}^{\mathrm{l}}, \ldots, w_{kL}^{\mathrm{l}}]^{\mathrm{T}}$ and $\mathbf{w}_k^{\mathrm{r}} = [w_{k1}^{\mathrm{r}}, \ldots, w_{kL}^{\mathrm{r}}]^{\mathrm{T}}$ denote the corresponding weight vectors of the beamformers. Similarly, $\mathbf{e}_k^{\mathrm{l}}(t) = [e_{k1}^{\mathrm{l}}(t), \ldots, e_{kL}^{\mathrm{l}}(t)]^{\mathrm{T}}$ and $\mathbf{e}_k^{\mathrm{r}}(t) = [e_{k1}^{\mathrm{r}}(t), \ldots, e_{kL}^{\mathrm{r}}(t)]^{\mathrm{T}}$ are the additive noise vectors of these two spatial filters. The outputs of these spatial filters become

$$y_k^{\mathrm{l}}(t) = \sum_{i=1}^{M} a_{ik}(t)\tilde{s}_i(t-\tau_{ik})e^{j2\pi(f_c(-\tau_{ik})+f_{\mathrm{D}ik}(t-\tau_{ik}))} \times (\mathbf{w}_k^{\mathrm{l}})^{\mathrm{H}}\mathbf{d}(\theta_k, f_c + f_{\mathrm{D}ik}) + (\mathbf{w}_k^{\mathrm{l}})^{\mathrm{H}}\mathbf{e}_k^{\mathrm{l}}(t) \tag{7}$$

$$y_k^{\mathrm{r}}(t) = \sum_{i=1}^{M} a_{ik}(t)\tilde{s}_i(t-\tau_{ik})e^{j2\pi(f_c(-\tau_{ik})+f_{\mathrm{D}ik}(t-\tau_{ik}))} \times (\mathbf{w}_k^{\mathrm{r}})^{\mathrm{H}}\mathbf{d}(\theta_k, f_c + f_{\mathrm{D}ik}) + (\mathbf{w}_k^{\mathrm{r}})^{\mathrm{H}}\mathbf{e}_k^{\mathrm{r}}(t). \tag{8}$$

Defining

$$x_k(t) \triangleq \sum_{i=1}^{M} a_{ik}(t)\tilde{s}_i(t-\tau_{ik})e^{j2\pi(f_c(-\tau_{ik})+f_{\mathrm{D}ik}(t-\tau_{ik}))} \tag{9}$$

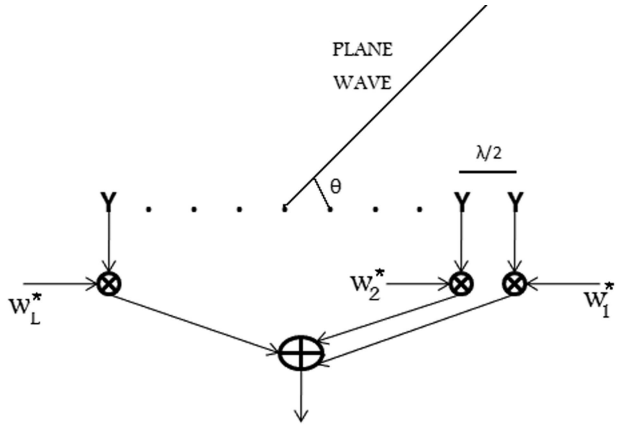

Fig. 4. Spatial beamformer at receiver.

we get the sampled outputs as

$$y_k^{\mathrm{l}}[n] = x_k[n](\mathbf{w}_k^{\mathrm{l}})^{\mathrm{H}}\mathbf{d}(\theta_k, f_{\mathrm{c}} + f_{\mathrm{D}ik}) + (\mathbf{w}_k^{\mathrm{l}})^{\mathrm{H}}\mathbf{e}_k^{\mathrm{l}}[n] \tag{10}$$

$$y_k^{\mathrm{r}}[n] = x_k[n](\mathbf{w}_k^{\mathrm{r}})^{\mathrm{H}}\mathbf{d}(\theta_k, f_{\mathrm{c}} + f_{\mathrm{D}ik}) + (\mathbf{w}_k^{\mathrm{r}})^{\mathrm{H}}\mathbf{e}_k^{\mathrm{r}}[n]. \tag{11}$$

We assume that the additive noise vectors at the two arrays of sensors have zero mean and covariance matrices $\mathbf{R}_k^{\mathrm{l}}$ and $\mathbf{R}_k^{\mathrm{r}}$, respectively. The Capon beamformer creates the beams by minimizing $(\mathbf{w}_k^{\mathrm{l}})^{\mathrm{H}}\mathbf{R}_k^{\mathrm{l}}\mathbf{w}_k^{\mathrm{l}}$ and $(\mathbf{w}_k^{\mathrm{r}})^{\mathrm{H}}\mathbf{R}_k^{\mathrm{r}}\mathbf{w}_k^{\mathrm{r}}$ subject to the constraints $\{(\mathbf{w}_k^{\mathrm{l}})^{\mathrm{H}}\mathbf{d}(\theta_k^{\mathrm{l}}, f_{\mathrm{c}}) = 1\}$ and $\{(\mathbf{w}_k^{\mathrm{r}})^{\mathrm{H}}\mathbf{d}(\theta_k^{\mathrm{r}}, f_{\mathrm{c}}) = 1\}$, respectively. The solution to this optimization problem gives the weights of the beamformers [39]

$$\mathbf{w}_k^{\mathrm{l}} = \frac{(\mathbf{R}_k^{\mathrm{l}})^{-1}\mathbf{d}(\theta_k^{\mathrm{l}}, f_{\mathrm{c}})}{\mathbf{d}(\theta_k^{\mathrm{l}}, f_{\mathrm{c}})^{\mathrm{H}}(\mathbf{R}_k^{\mathrm{l}})^{-1}\mathbf{d}(\theta_k^{\mathrm{l}}, f_{\mathrm{c}})} \tag{12}$$

$$\mathbf{w}_k^{\mathrm{r}} = \frac{(\mathbf{R}_k^{\mathrm{r}})^{-1}\mathbf{d}(\theta_k^{\mathrm{r}}, f_{\mathrm{c}})}{\mathbf{d}(\theta_k^{\mathrm{r}}, f_{\mathrm{c}})^{\mathrm{H}}(\mathbf{R}_k^{\mathrm{r}})^{-1}\mathbf{d}(\theta_k^{\mathrm{r}}, f_{\mathrm{c}})} \tag{13}$$

where θ_k^{l}, θ_k^{r} are the angles at which both the beams are directed. Hence, boresight axis of the receiver is located at an angle $\theta_k^{\mathrm{b}} = (\theta_k^{\mathrm{l}} + \theta_k^{\mathrm{r}})/2$. In practice, the covariance matrices $\mathbf{R}_k^{\mathrm{l}}$ and $\mathbf{R}_k^{\mathrm{r}}$ are not known at the receiver a priori. Therefore, they are approximated using the sample covariance matrices $\widehat{\mathbf{R}_k^{\mathrm{l}}}$ and $\widehat{\mathbf{R}_k^{\mathrm{r}}}$, respectively.

In Fig. 5, we plotted the response of the two spatial filters to exponential signals of frequency f_{c} coming from different angles. The left and the right beams are designed for signals coming from angles 80 deg and 75 deg, respectively with a frequency f_{c}. Hence, the boresight axis is at an angle of 77.5 deg. We used an array of 10 elements to generate these beams and the beams were designed for a diagonal covariance matrix with a variance of 0.1 for the measurements. The response of these spatial filters at the boresight angle is 0.9258. We can control the widths of each of these beams by adjusting the number of elements in the linear array. A larger value of L gives a narrower beamwidth because of the increased degrees of freedom.

We evaluate the sum and the difference of the absolute values of the complex outputs at the two beamformers

$$y_k^{\mathrm{s}}[n] = \mathrm{abs}\{y_k^{\mathrm{l}}[n]\} + \mathrm{abs}\{y_k^{\mathrm{r}}[n]\} \tag{14}$$

$$y_k^{\mathrm{d}}[n] = \mathrm{abs}\{y_k^{\mathrm{l}}[n]\} - \mathrm{abs}\{y_k^{\mathrm{r}}[n]\} \tag{15}$$

where the superscripts s and d denote the sum and difference channels, respectively; abs$\{\cdot\}$ represents the absolute value of the complex number in the argument. Now, we send the measurements from these two channels to the monopulse processor for

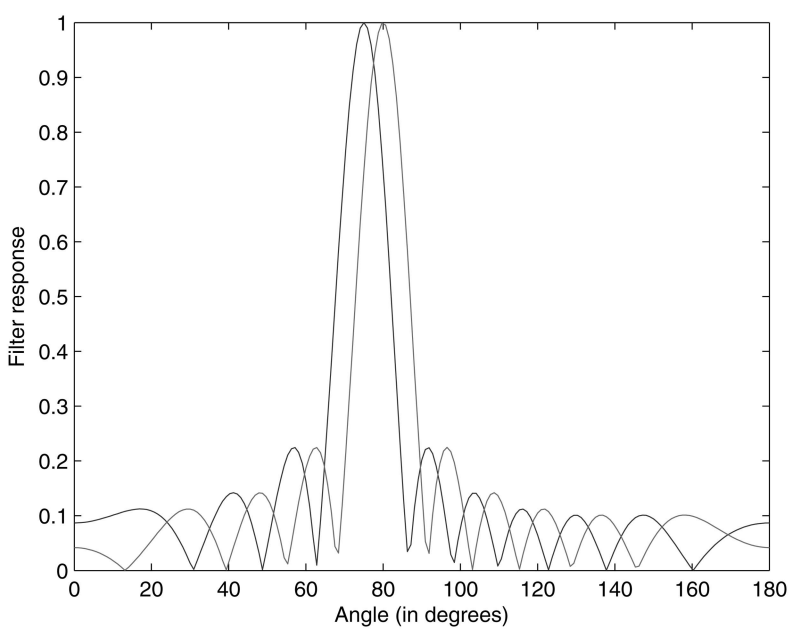

Fig. 5. Responses of two spatial filters as a function of the angle.

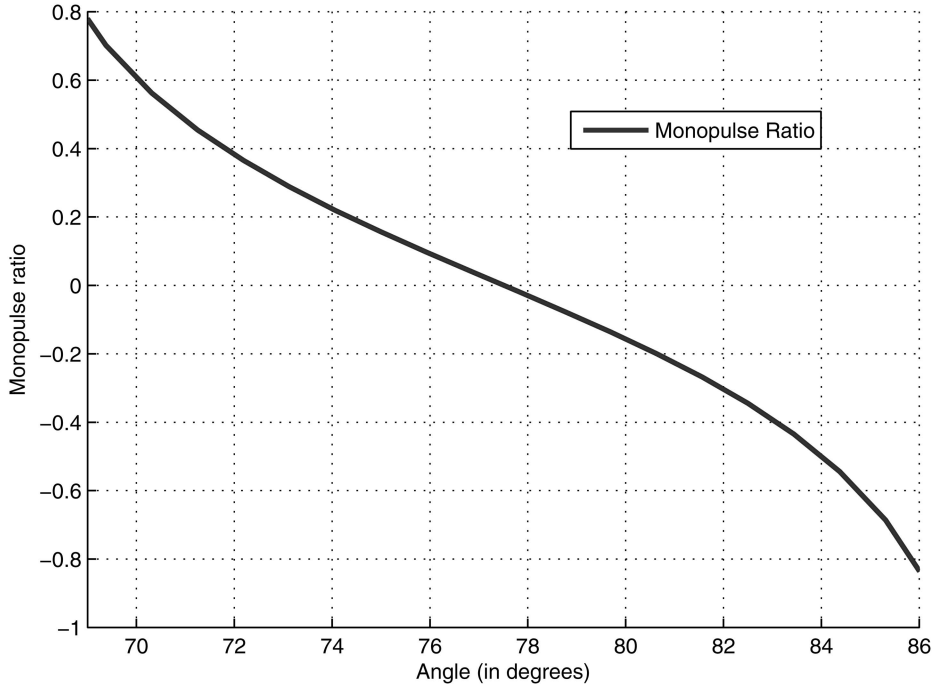

Fig. 6. Monopulse ratio as a function of the angle.

the decision making about the angular location of the target.

IV. TRACKING ALGORITHM

We propose a tracking algorithm for monopulse MIMO radar in this section.

A. Initialization

The fusion center has the information about the exact locations of all the receivers. It will initialize the tracking algorithm by making sure that the boresight axes of all the receivers intersect at the same point in space. After this, the receivers obtain the measurements from the first pulse according to (10) and (11).

B. Monopulse Processing. Local Angular Estimates

After obtaining the measurements from the sum and the difference channels, each of the receivers computes the monopulse ratio

$$M_k[n] = \frac{y_k^{\mathrm{d}}[n]}{y_k^{\mathrm{s}}[n]}. \tag{16}$$

If the $M_k[n]$ is positive, it implies that it is highly likely for the target to be present on the left side of the boresight axis. Similarly, a negative $M_k[n]$ indicates the opposite. The receiver k will adjust its boresight axis appropriately using the following equation

$$\theta_k^{\mathrm{b(new)}} = \theta_k^{\mathrm{b}} + \delta\{M_k[n]\} \tag{17}$$

where δ is a positive valued design parameter. The above equation essentially increases the value of θ_k^{b} if the target is present to the left side of the axis and reduces it if the target is on the other side. The amount of increase or decrease in the angular adjustment is proportional to the monopulse ratio. The parameter δ has to be chosen carefully. A larger value of δ will enable tracking faster moving targets but will also lead to higher steady state errors. However, a smaller δ will increase the convergence time but the steady state errors will be less. Each of the receivers updates its angular estimates using the above mentioned processing. In our proposed system, we adjust the boresight axes electronically by adjusting the weights of both the beamformers. However, we can also do this by mechanically steering both the beams. The disadvantage of using mechanical steering is the delay encountered while rotating the beams. Electronic steering by beamforming is very quick and can be done instantaneously by adjusting the weights appropriately.

In Fig. 6 we plot the monopulse ratio formed by using the two spatial filters shown in Fig. 5. It can be seen that the ratio changes its sign exactly at the middle point between the two beams, i.e., 77.5 deg. The beams that we used in our numerical results have exactly the same width and same separation angle as mentioned in this example.

C. Fusion Center. Global Location Estimate

The primary function of the fusion center is to combine these decentralized estimates and arrive at a global estimate for the target location. We have solved a similar problem for localizing acoustic sources using

TABLE I
Tracking Algorithm

Step 1:	Fusion center directs all the receivers to align their boresight axes to the same location.
Step 2:	Each receiver calculates $M_k[n]$ and adjusts boresight axis to $\theta_k^{\mathrm{b(new)}} = \theta_k^{\mathrm{b}} + \delta\{M_k[n]\}$.
Step 3:	Receivers send $\theta_k^{b(\mathrm{new})}$ and $E_k[n] = (y_k^{\mathrm{s}}[n])^2$ to the fusion center.
Step 4:	Fusion center identifies the points of intersection of these axes $(p_{x_{ij}}[n], p_{y_{ij}}[n])$ and estimates the target location to be $(\widehat{p_x}[n], \widehat{p_y}[n]) = \sum_{i=1}^{N}\sum_{j=i+1}^{N} \alpha_{ij}[n](p_{x_{ij}}[n], p_{y_{ij}}[n])$, where $\alpha_{ij}[n] = \left(E_i[n] + E_j[n]\right) \Big/ \left(\sum_{i'=1}^{N}\sum_{j'=i'+1}^{N}(E_{i'}[n] + E_{j'}[n])\right)$.
Step 5:	Fusion center directs all the receivers to point their boresight axes to this new estimate $(\widehat{p_x}[n], \widehat{p_y}[n])$ and we start again with step 2.

Cramer-Rao bound [40]. Here, we present a simpler method to combine the decentralized estimates. After obtaining new angular estimates, each of the receivers sends these new updates to the fusion center. Along with the angular estimates, the receivers also send the instantaneous energy of the received signal in the sum channel during that instant.

$$E_k[n] = (y_k^{\mathrm{s}}[n])^2. \tag{18}$$

The fusion center forms a polygon of $N(N-1)/2$ sides by connecting the points of intersection of the updated boresight axes of each of the N receivers (see Fig. 7). See also [26]. The fusion center will decide upon a point inside this polygon to be the global estimate of the target location. Define $(p_{x_{ij}}[n], p_{y_{ij}}[n])$ to be the Cartesian coordinates of the vertex formed by the intersection of the boresight axes coming out from the ith receiver and the jth receiver. A linear combination of these vertices is chosen as the estimate of the target location

$$(\widehat{p_x}[n], \widehat{p_y}[n]) = \sum_{i=1}^{N}\sum_{j=i+1}^{N} \alpha_{ij}[n](p_{x_{ij}}[n], p_{y_{ij}}[n]). \tag{19}$$

We choose the weights $\alpha_{ij}[n]$ to be proportional to the sum of instantaneous energies received from the corresponding receivers and $\sum_{i=1}^{N}\sum_{j=i+1}^{N} \alpha_{ij}[n] = 1$. Therefore,

$$\alpha_{ij}[n] = \frac{E_i[n] + E_j[n]}{\sum_{i'=1}^{N}\sum_{j'=i'+1}^{N}(E_{i'}[n] + E_{j'}[n])}. \tag{20}$$

These weights also depend on the locations of the transmitters and receivers relative to the target. The signal at each receiver is a sum of the signals coming from different transmitters and bouncing off the surface of the target. Therefore, the path length and the target RCS play an important role in determining the received energies. Hence, it is highly likely that a transmitter-receiver pair which has a good look at the target and shorter path length will give a significant contribution to the instantaneous received energy at that receiver.

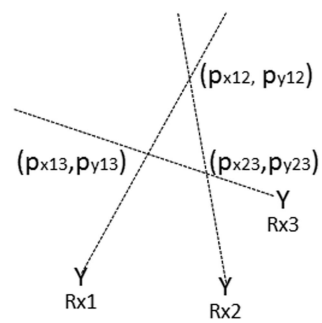

Fig. 7. Polygon formed by points of intersection of boresight axes of three receivers.

Finally, the fusion center sends the new estimate $(\widehat{p_x}[n], \widehat{p_y}[n])$ to all the receivers and guides them to align their axes towards this particular location before the next iteration. We summarize the important steps of the algorithm in Table I. Note that the Doppler frequencies that appear in the expressions for the received measurements (see Section III) will degrade the performance of the tracking algorithm because they also impact the computation of the monopulse ratio and these frequencies are not known at the receivers. However, in certain situations, having large Doppler shifts might be an advantage. Consider an example when there is an additional target close to the target of interest. In such a scenario, if these targets have significantly different Doppler frequencies, we can separate the signals from both of them using Doppler filters if we have a rough estimate of these frequencies. Therefore, in such situations, it is useful if the Doppler shifts of the targets are far apart.

D. Multiple Targets

The scenario in which multiple targets are present in the illuminated scene is of interest. If we have more than a single target, the tracking algorithm might end up pointing towards neither of the actual targets. It could be pointing towards some region in between these targets. The multi-target problem has been addressed in [41]–[46]. Reference [41] studies the varieties of monopulse responses to multiple targets. The problem of estimation of the direction

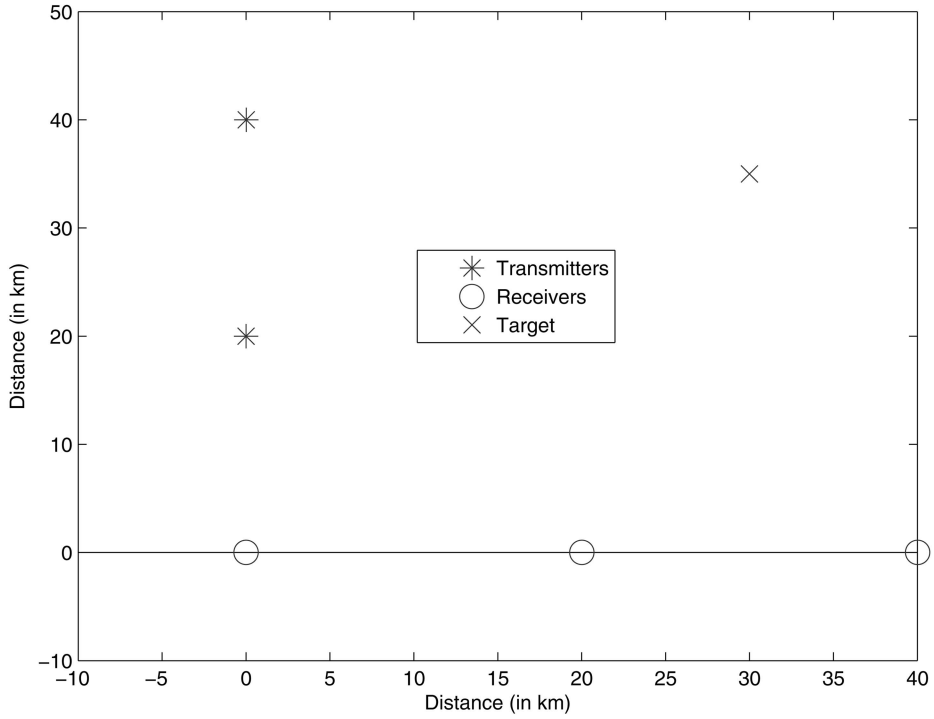

Fig. 8. Simulated radar-target scenario.

of arrival is studied in [43], in the context of two unresolved Rayleigh targets. In [45], the authors exploit the Doppler separation between the targets to perform the tracking of the intended target in the presence of the interfering target. These different techniques can be applied at each of the receivers in our proposed system. Also, we use electronic steering for rotating the beams at the receivers. Hence, this can be done instantaneously without much delay. This is in contrast with mechanical steering that will have some lag. This helps us to continue to keep track of the multiple moving targets even when they move into different range bins. We can quickly switch the receive beams from one angle to another as we move from one range bin to another. Thus, the point of intersection of the boresight axes of the receivers (see Fig. 3) can be made to change from one range bin to another. Also, we can apply Doppler processing to separate the targets in a similar manner as it is done for SISO monopulse radar.

V. NUMERICAL RESULTS

A. Simulated Scenario

In this section, we demonstrate the advantage of the proposed monopulse MIMO tracking system under realistic scenarios. We simulated such a scenario to demonstrate the advantages of this system. First we describe the locations of the transmitters, receivers, and target on a Cartesian coordinate system. The simulated system has two transmitters that are located on the y-axis at distances of 20 km and 40 km from the origin, respectively. There are three receivers located on the x-axis at the origin, 20 km and 40 km from the origin, respectively. The receiver at the origin also serves as the fusion center for this setup. The target is initially present at the coordinate (30,35). Fig. 8 shows the simulated radar-target scenario.

We chose the carrier frequency $f_c = 1$ GHz. We used complex rectangular pulses each with a constant value $(1+\sqrt{-1})/\sqrt{2}$ and bandwidth 100 MHz for the transmitted baseband waveforms. Therefore, the pulse duration $T = 10^{-8}$ s. The pulses coming from different transmitters reach the receivers in different intervals of time because of the different delays caused by the distances between them. The processing remains the same even if the square pulses from different transmit antennas overlap because we are only interested in the ratio of the signals in the difference and the sum channels, i.e., we do not need a mechanism to separate these pulses. The pulse repetition interval $T_R = 4$ ms. We further had two samples per pulse duration (Nyquist rate). We ran the simulation for 2 s. Hence, we had 500 pulses from each transmitter. The target is airborne and moving with a constant velocity of (0.25,0.25) km/s. There are six complex numbers $\{a_{11}, a_{12}, a_{13}, a_{21}, a_{22}, a_{23}\}$ describing the attenuation experienced by the signals. It is important to realistically model these attenuations. They were independently generated from one pulse to another using zero mean complex normal random variables with their variances chosen from the set $\{0.15, 0.3, 0.45, 0.6, 0.75, 0.9\}$. The a_{ik} corresponding

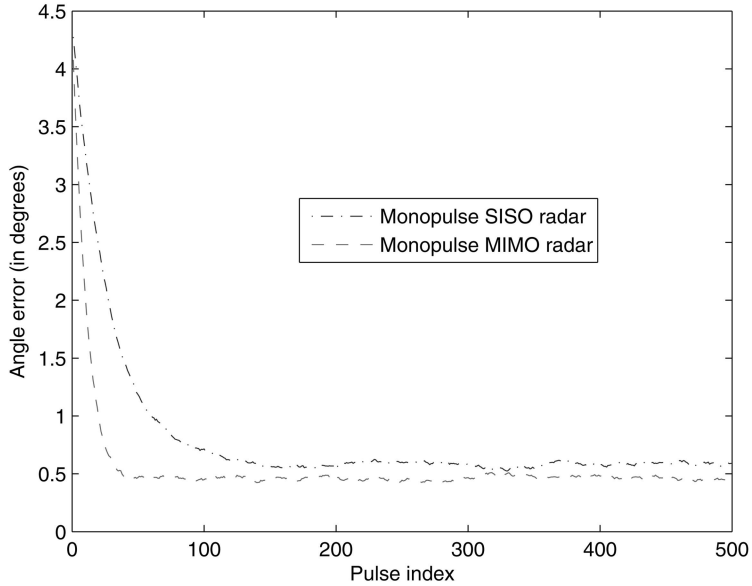

Fig. 9. Comparing angle error of SISO and MIMO monopulse radars as function of pulse index for $\sigma^2 = 0.1$.

to the antenna pair that are the closest to the target got the higher values and vice versa. We assumed the additive noise at every element of the receiver array is uncorrelated zero mean complex Gaussian distributed with variance σ^2. The received powers are different at different receivers because the attenuations a_{ik} do not have the same variances. Therefore, we evaluate the overall signal-to-noise ratio (SNR) by computing the average. For a noise variance of $\sigma^2 = 0.1$, SNR = 12.3 dB. We further assumed the noise to be stationary. The noise variance was estimated from a training data set of 50 samples. We assumed that the target returns were not present in the training samples that were used. We independently generated the noise from one time sample to another. The two beams at each receiver were generated using $L = 10$ element linear arrays and they were made to point 5 deg on either side of the boresight axis. The -3 dB beamwidth of these beams is approximately 12 deg. We chose the parameter $\delta = 0.25$ deg in our algorithm.

B. Spatial Diversity

We first demonstrate the spatial diversity offered by monopulse MIMO radar with widely separated antennas by comparing this system with monopulse SISO radar. Since a single receiver monopulse tracking radar can only track the angular location of the target, we compare only the angle errors of the SISO and MIMO monopulse radars. For SISO radar, we assumed only the first transmitter $(0,20)$ and the first receiver $(0,0)$ (see Fig. 8) to be present. First, we assumed that the initial estimate of the target location for 2×3 MIMO radar is far from the actual location at $(32,32)$. Hence, the initial estimate was at a distance of 3.61 km from the actual location. The same initial estimate was also used for SISO radar and it corresponds to an initial angular error of 4.3987 deg. In order to make the comparison fair, we deliberately increased the transmit power per antenna for the SISO system to make the overall transmit power the same. We chose the complex noise variance σ^2 for this comparison to be 0.1. We plotted the angular error as a function of the pulse index. Fig. 9 shows that the MIMO system overcomes a poor initial estimate and manages to track down the target much quicker than the SISO radar. The SISO system takes 60 pulses to come within an angular error of 1 degree. However, the 2×3 MIMO system takes only 20 pulses to reach within the same level of angular error. To obtain good accuracy, we plotted these curves by averaging the results over 100 independent realizations.

Next, we assumed a good initial estimate of $(29.9,34.9)$ and plotted the average angular errors of both these systems as a function of the complex noise variances. As expected, Fig. 10 shows that the average angular error increases with an increase in the noise variance. MIMO system significantly outperforms the SISO system. The angular error of these systems can further be reduced by using a smaller value of δ. However, if the initial estimate of the target location is poor, a smaller δ would mean that the convergence time of the algorithm would increase. Hence, it is a trade-off between the steady-state error and convergence rate. Note that as the noise variance reduces, the gap between the performances of the systems reduces because the advantage offered by the spatial diversity becomes more relevant when there is more noise. The performance of any monopulse system is independent of the absolute values of the signals of interest. This is an outcome of the fact that we use a ratio in monopulse processing instead of the absolute values of the measured signals in both

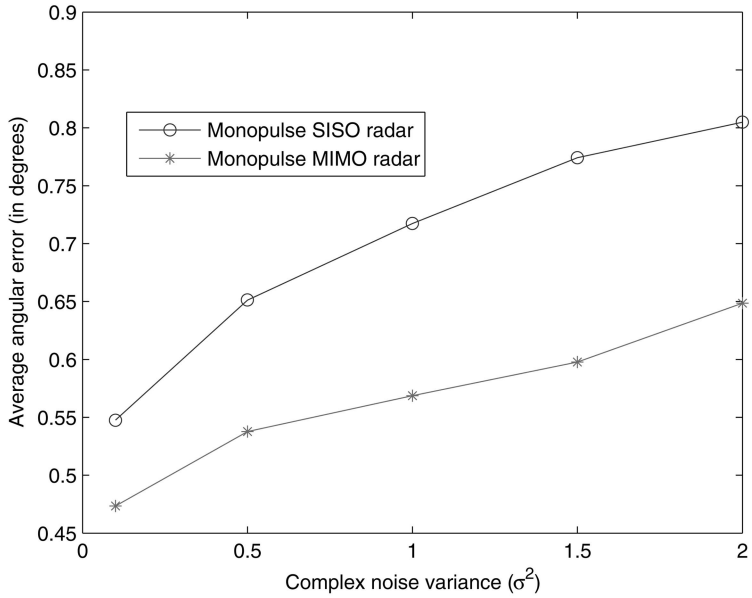

Fig. 10. Comparing average angle error of SISO and MIMO monopulse radars as function of complex noise variance σ^2.

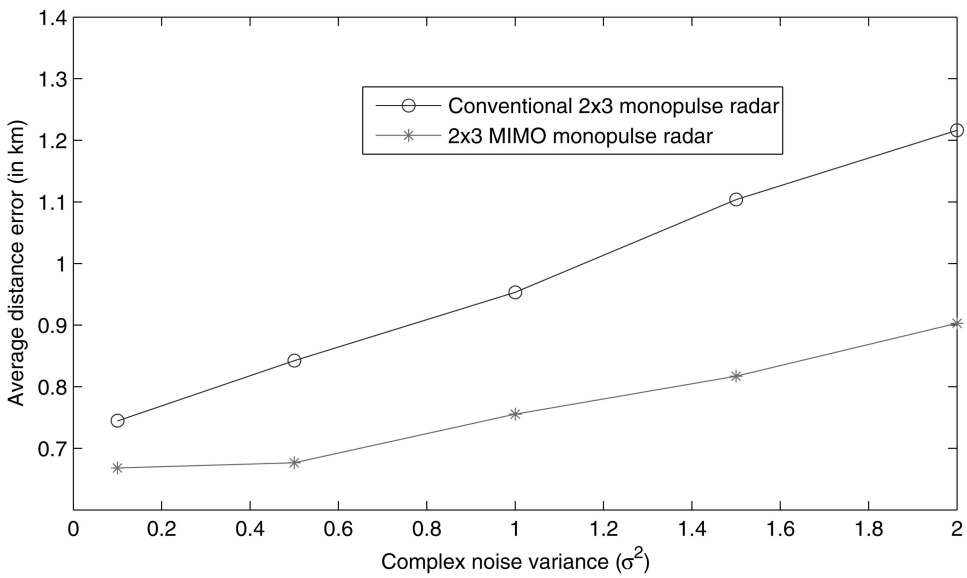

Fig. 11. Comparing average distance errors of 2×3 MIMO and conventional radars as function of complex noise variance σ^2.

the channels. As the noise variance increases, we get to see that the improvement offered by the spatial diversity of the MIMO system also increases.

The advantage of the proposed monopulse MIMO radar over monopulse SISO radar stems from the fact that by employing multiple antennas, we are exploiting the fluctuations in the target RCS values with respect to the angle of view. Even if the RCS between one transmitter-receiver pair is very small, it is highly likely that the other transmitter-receiver pairs will compensate for it. Also, in our proposed algorithm, the weights are proportional to the received energies. Hence, with high probability, a transmitter-receiver pair with high RCS value will contribute significantly to the received energy at that particular receiver.

Along with tracking the angular location of the target, the exact coordinates of the target location can also be estimated by evaluating the points of intersection of the boresight axes coming from all the receivers. Since this processing is possible only for monopulse systems with multiple receivers, we compare the the locating capabilities of our proposed 2×3 MIMO radar and conventional 2×3 radar. For the conventional 2×3 radar, all the 6 attenuations will be the same whereas these attenuations will be different for MIMO radar due to the wide antenna separation. This takes care of the target fluctuations. From Fig. 11, it is evident that MIMO radar outperforms the conventional 2×3 radar at all the noise variances since it offers more spatial diversity.

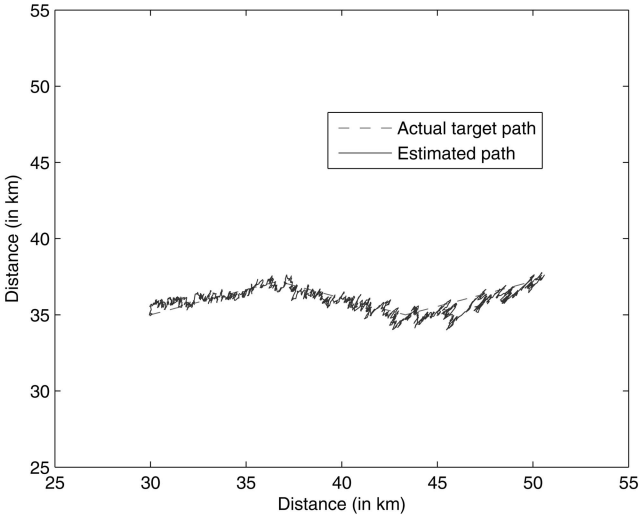

Fig. 12. Monopulse MIMO tracker for rapidly maneuvering airborne target for $\sigma^2 = 0.1$.

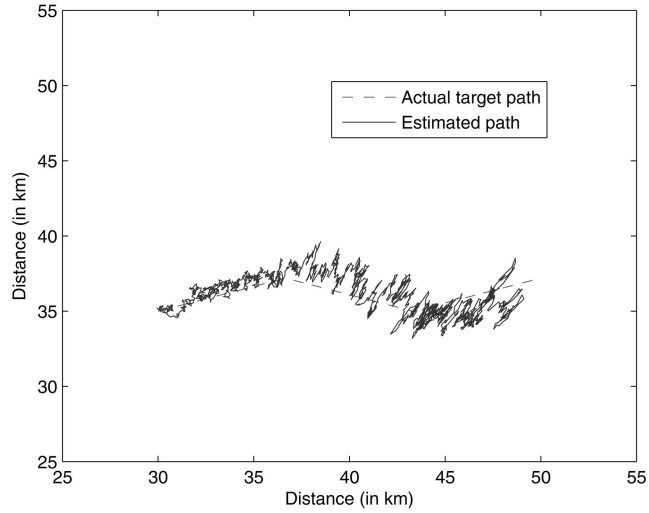

Fig. 13. Monopulse MIMO tracker for rapidly maneuvering airborne target in presence of jammer for $\sigma^2 = 0.1$.

In the following simulations, we show the localizing abilities of 2×3 MIMO radar under different challenging scenarios.

C. Rapidly Maneuvering Airborne Target

A clever target would change its direction of travel at high velocities to reduce the detectability and to confuse the tracking radar. Hence, it is extremely important to track a rapidly maneuvering airborne target. In order to check the performance of the algorithm in this scenario, we increased the velocity of the target to $(2.5, 0.833)$ km/s and further made the target change its direction at two different locations over a time span of 8 s. These high velocities are a feature of the next generation hypersonic missiles. We see from Fig. 12 that the radar system keeps track of the target inspite of the very high velocities and direction changes. The noise variance $\sigma^2 = 0.1$ for this simulation. This corresponds to an SNR of 12.3 dB.

D. Effect of a Jamming Signal

In defense applications, the enemy tries to mislead the radar by sending jamming signals that interfere with the target returns. If the frequency of the jamming signals is close to f_c, it is difficult for the radar to localize the target. This situation is analogous to having an interfering target apart from the target of interest. We now show that the proposed monopulse MIMO radar system manages to locate the target even in the presence of a jamming sinusoid of frequency f_c. We assumed the source of the sinusoid to be located at the coordinates $(25, 10)$. We chose the power of the received sinusoid to be 10 percent of that of each transmitted waveform. We used the same target path and velocities as described for the rapidly maneuvering airborne target. We clearly see from Fig. 13 that there is a degradation in performance when compared with Fig. 12 because of the jamming signal. The tracker moves in a different direction for a while but still manages to correct itself and locate the target. Hence, even in the presence of the jammer, the proposed system manages to follow a rapidly maneuvering airborne target.

E. Sequential versus Simultaneous Lobing

We mentioned in the Introduction section that simultaneous lobing (monopulse) is immune to pulse-to-pulse fluctuations whereas sequential lobing suffers from this drawback. Now we demonstrate the advantage of choosing simultaneous lobing for our proposed system using numerical simulations. We used the same radar, rapidly maneuvering airborne target, and jammer scenario as described in this section. In order to make a fair comparison, we doubled the pulse repetition frequency for sequential lobing to keep the overall data rate constant. It is evident from Fig. 14 that the system completely loses track of the target in the middle of the flight. It moves in a completely different direction to that of the target. In fact, the tracker moves significantly in the direction of the jamming source located at $(25, 10)$. This shows the shortcomings of sequential lobing and thus emphasizes the advantages of using monopulse for the proposed multiple antenna tracking radar.

F. Maneuvering Ground Target

Ground targets move at lesser velocities when compared with the airborne targets we have considered so far. However, ground targets have the flexibility to change directions at sharp angles. They can sometimes change their direction by 90 deg. This poses an important challenge to the tracking system. In Fig. 15, we simulated a ground target moving at

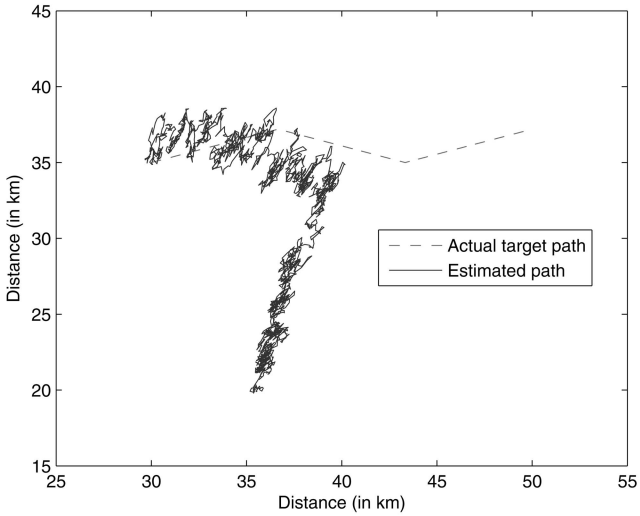

Fig. 14. Monopulse MIMO tracker for rapidly maneuvering airborne target using sequential lobing in presence of jammer for $\sigma^2 = 0.1$.

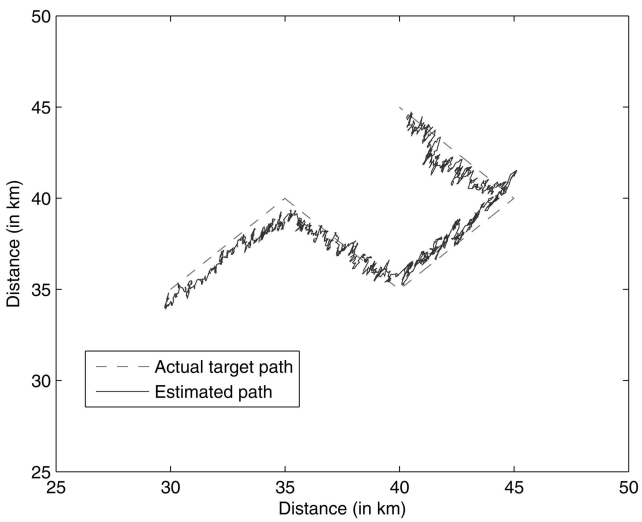

Fig. 15. Monopulse MIMO tracker for a maneuvering ground target for $\sigma^2 = 0.1$.

a velocity of (25, 25) m/s and completely changing directions at three different locations. Since the target moves slower than an airborne target, we chose the pulse repetition rate $T_R = 0.4$ s for the simplicity of numerical simulations. We see that the tracker follows the target at each of these locations inspite of the sharp angle changes and the reduction of pulse repetition frequency.

VI. CONCLUSION

We have proposed a multiple distributed antenna tracking radar system with monopulse receivers. We used Capon beamforming to generate the beams of the monopulse receivers. Further, we developed a tracking algorithm for this system. We simulated a realistic scenario to analyze the performance of the proposed system. We demonstrated the advantages offered by this system over conventional single antenna monopulse tracking radar. This advantage is a result of the spatial diversity offered by distributed MIMO radar systems. We also showed that the proposed system keeps track of a rapidly maneuvering airborne target, even in the presence of an intentional jamming signal. This is an extremely important feature in any defence application. Further, we demonstrated the advantages of having simultaneous lobing (monopulse) in our system as opposed to sequential lobing. Also, we showed that the monopulse MIMO tracker follows a maneuvering ground target that changes its directions at sharp angles.

In future work, we will perform an asymptotic error analysis and develop performance bounds for the proposed tracking algorithm. We will also use real data to demonstrate the advantages of the proposed system.

SANDEEP GOGINENI
ARYE NEHORAI
Dept. of Electrical and Systems Engineering
Washington University in St. Louis
One Brookings Drive
St. Louis, MO 63130
E-mail: (sgogineni@ese.wustl.edu)

REFERENCES

[1] Haimovich, A. M., Blum, R. S., and Cimini, L. J. MIMO radar with widely separated antennas. *IEEE Signal Processing Magazine*, **25** (Jan. 2008), 116–129.

[2] Li, J. and Stoica, P. *MIMO Radar Signal Processing*. Hoboken, NJ: Wiley, 2009.

[3] He, Q., Blum, R. S., Godrich, H., and Haimovich, A. M. Cramer-Rao bound for target velocity estimation in MIMO radar with widely separated antennas. In *Proceedings of the 42nd Annual Conference on Information Sciences and Systems*, Princeton, NJ, Mar. 2008, 123–127.

[4] Gogineni, S. and Nehorai, A. Polarimetric MIMO radar with distributed antennas for target detection. *IEEE Transactions on Signal Processing*, **58** (Mar. 2010), 1689–1697.

[5] Fishler, E., Haimovich, A. M., Blum, R. S., Cimini, Jr., L. J., Chizhik, D., and Valenzuela, R. A. Spatial diversity in radars—Models and detection performance. *IEEE Transactions on Signal Processing*, **54** (Mar. 2006), 823–838.

[6] Akcakaya, M., Hurtado, M., and Nehorai, A. MIMO radar detection of targets in compound-Gaussian clutter. In *Proceedings of the 42nd Asilomar Conference on Signals, Systems and Computers*, Pacific Grove, CA, Oct. 2008, 208–212.

[7] Gogineni. S. and Nehorai, A. Polarimetric MIMO radar with distributed antennas for target detection. In *Proceedings of the 43rd Asilomar Conference on Signals, Systems and Computers*, Pacific Grove, CA, Nov. 2009, 1144–1148.

[8] Li, J. and Stoica, P.
MIMO radar with colocated antennas.
IEEE Signal Processing Magazine, **24** (2007), 106–114.

[9] Li, J., Stoica, P., Xu, L., and Roberts, W.
On parameter identifiability of MIMO radar.
IEEE Signal Processing Letters, **14** (Dec. 2007), 968–971.

[10] Skolnik, M.
Radar Handbook.
Columbus, OH: Mcgraw-Hill, 2008.

[11] Rhodes, D. R.
Introduction to Monopulse.
New York: McGraw-Hill, 1959.

[12] Sherman, S. M.
Monopulse Principles and Techniques.
Dedham, MA: Artech House, 1985.

[13] Groves, G. W., Blair, W. D., and Chow, W. C.
Probability distribution of complex monopulse ratio with arbitrary correlation between channels.
IEEE Transactions on Aerospace and Electronic Systems, **33** (Oct. 1997), 1345–1350.

[14] Blair, W. D. and Brandt-Pearce, M.
Statistical description of monopulse parameters for tracking Rayleigh targets.
IEEE Transactions on Aerospace and Electronic Systems, **34** (Apr. 1998), 597–611.

[15] Kanter, I.
The probability density function of the monopulse ratio for N looks at a combination of constant and Rayleigh targets.
IEEE Transactions on Information Theory, **IT-23** (Sept. 1977), 643–648.

[16] Kanter, I.
Three theorems on the moments of the monopulse ratio.
IEEE Transactions on Information Theory, **IT-24** (Mar. 1978), 272–276.

[17] Willett, P. K., Blair, W. D., and Bar-Shalom, Y.
Correlation between horizontal and vertical monopulse measurements.
IEEE Transactions on Aerospace and Electronic Systems, **39** (Apr. 2003), 533–549.

[18] Sinsky, A. I. and Lew, E. A.
Comparative analysis of a phase and an amplitude processor for amplitude monopulse system.
IEEE Transactions on Antennas and Propagation, **AP-31** (May 1983), 519–522.

[19] Endo, T.
Analysis of interference effects on monopulse radars.
IEEE Transactions on Aerospace and Electronic Systems, **24** (Nov. 1988), 766–774.

[20] Seifer, A. D.
Monopulse-radar angle tracking in noise or noise jamming.
IEEE Transactions on Aerospace and Electronic Systems, **28** (July 1992), 622–638.

[21] Blair, W. D. and Brandt-Pearce, M.
Unresolved Rayleigh target detection using monopulse measurements.
IEEE Transactions on Aerospace and Electronic Systems, **34** (Apr. 1998), 543–552.

[22] Nandakumaran, N., Sinha, A., and Kirubarajan, T.
Joint detection and tracking of unresolved targets with monopulse radar.
IEEE Transactions on Aerospace and Electronic Systems, **44** (Oct. 2008), 1326–1341.

[23] Nickel, U.
Overview of generalized monopulse estimation.
IEEE Aerospace and Electronic Systems Magazine, **21** (June 2006), 27–56.

[24] Roberts, J. H.
Analysis of interference effects on monopulse radars.
IET Electronics Letters, **20** (Apr. 1984), 382–383.

[25] Rainal, A. J.
Monopulse radars excited by Gaussian signals.
IEEE Transactions on Aerospace and Electronic Systems, **AES-2** (May 1966), 337–345.

[26] Mao, G., Fidan, B., and Anderson, B.
Wireless sensor network localization techniques.
Computer Networks, **51** (July 2007), 2529–2553.

[27] Oshman, Y. and Davidson, P.
Optimization of observer trajectories for bearings-only target localization.
IEEE Transactions on Aerospace and Electronic Systems, **35** (July 1999), 892–902.

[28] Bishop, A. N., Fidan, B., Anderson, B. D. O., Dogancay, K., and Pathirana, P. N.
Optimality analysis of sensor-target geometries in passive localization: Part 1—Bearing-only localization.
In *Proceedings of the 3rd International Conference on Intelligent Sensors, Sensor Networks and Information Processing* (ISSNIP), Melbourne, VIC, Australia, Dec. 2007, 7–12.

[29] Bar-Shalom, Y., Li, X. R., and Kirubarajan, T.
Estimation with Applications to Tracking and Navigation: Theory, Algorithms, and Software.
New York: Wiley, 2001.

[30] Gogineni, S. and Nehorai, A.
Target tracking using monopulse MIMO radar with distributed antennas.
In *Proceedings of the 2010 IEEE International Radar Conference*, Washington, D.C., May 2010, 194–199.

[31] Swerling, P.
Probability of detection for fluctuating targets.
IRE Transactions on Information Theory, **2** (Apr. 1960), 269–308.

[32] Mcnolty, F. and Hansen, E.
Some aspects of Swerling models for fluctuating radar cross section.
IEEE Transactions on Aerospace and Electronic Systems, **AES-10** (Mar. 1974), 281–285.

[33] Shnidman, D. A.
Expanded Swerling target models.
IEEE Transactions on Aerospace and Electronic Systems, **39** (July 2003), 1059–1069.

[34] Kelly, E. J.
The radar measurement of range, velocity and acceleration.
IRE Transactions on Military Electronics, **5** (Apr. 1961), 1–57.

[35] Kelly, E. J. and Wishner, R. P.
Matched-filter theory for high-velocity accelerating targets.
IEEE Transactions on Military Electronics, **MIL-9** (Jan. 1965), 56–69.

[36] Rihaczek, A.
Radar resolution of moving targets.
IEEE Transactions on Information Theory, **IT-13** (Jan. 1967), 51–56.

[37] Rihaczek, A.
Delay-Doppler ambiguity functions for wideband signals.
IEEE Transactions on Aerospace and Electronic Systems, **AES-3** (July 1967), 705–711.

[38] Capon, J.
High-resolution frequency-wavenumber spectrum analysis.
Proceedings of the IEEE, **57** (Aug. 1969), 1408–1418.

[39] Krim, H. and Viberg, M.
Two decades of array signal processing research.
IEEE Signal Processing Magazine, **13** (July 1996), 67–94.

[40] Hawkes, M. and Nehorai, A.
Wideband source localization using a distributed acoustic vector-sensor array.
IEEE Transactions on Signal Processing, **5** (June 2003), 1479–1491.

[41] Kanter, I.
Varieties of average monopulse responses to multiple targets.
IEEE Transactions on Aerospace and Electronic Systems, **AES-17** (Jan. 1981), 25.

[42] Howell, J. M.
Tracking performance of a monopulse radar in the presence of multiple targets.
IEEE Transactions on Aerospace and Electronic Systems, **AES-6** (Sept. 1970), 718.

[43] Blair, W. D. and Brandt-Pearce, M.
Monopulse DOA estimation of two unresolved Rayleigh targets.
IEEE Transactions on Aerospace and Electronic Systems, **37** (Apr. 2001), 452–469.

[44] Zhang, X., Willett, P. K., and Bar-Shalom, Y.
Monopulse radar detection and localization of multiple unresolved targets via joint bin processing.
IEEE Transactions on Signal Processing, **53** (Apr. 2005), 1225–1236.

[45] Kliger, I. E. and Olenberger, C. F.
Multiple target effects on monopulse signal processing.
IEEE Transactions on Aerospace and Electronic Systems, **AES-11** (Sept. 1975), 795–804.

[46] Gini, F., Greco, M., and Farina, A.
Multiple radar targets estimation by exploiting induced amplitude modulation.
IEEE Transactions on Aerospace and Electronic Systems, **39** (Oct. 2003), 1316–1332.